CRediT author statement:

Zipeng Liu: Methodology, Validation, Formal analysis, Investigation, Data Curation, Writing - Original Draft, Visualization. **Ling Chen:** Writing - Review & Editing, Conceptualization, Methodology, Resources, Supervision, Project administration, Funding acquisition. Writing - Review & Editing. **Pingping Bie**: Methodology, Writing - Review & Editing. **Fengwei Xie**: Methodology, Resources, Writing - Review & Editing, Visualization. **Bo Zheng:** Writing - Review & Editing, Conceptualization, Methodology, Resources, Supervision, Project administration.

Graphical Abstract
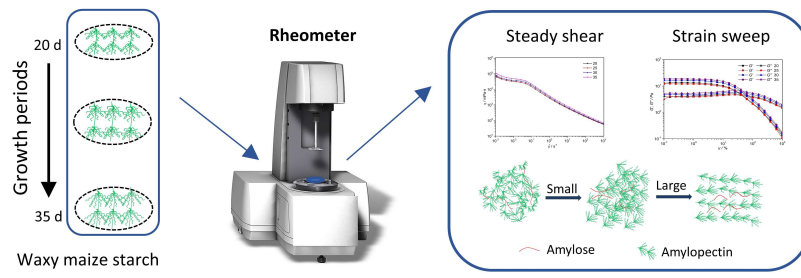
1 **An insight into the structural evolution of waxy maize starch**

2 **chains during growth based on nonlinear rheology**

3

4 Zipeng Liu [a], Ling Chen [a,**], PingPing Bie [a], Fengwei Xie [b, c], Bo Zheng [a,*]

5 *[a] Ministry of Education Engineering Research Center of Starch & Protein Processing, Guangdong*

6 *Province Key Laboratory for Green Processing of Natural Products and Product Safety, School of Food*

7 *Science and Engineering, South China University of Technology, Guangzhou 510640, China*

8 *[b] International Institute for Nanocomposites Manufacturing (IINM), WMG, University of*

9 *Warwick, Coventry CV4 7AL, United Kingdom*

10 *[c] School of Chemical Engineering, The University of Queensland, Brisbane, Qld 4072, Australia*

11

12 *Corresponding author. Email: bzheng@scut.edu.cn; (B. Zheng);

13 **Corresponding author. Email: felchen@scut.edu.cn; (L. Chen)

14

15 **Abbreviations**

16 WMS, waxy maize starch; NMR, nuclear magnetic resonance; GPC, gel permeation

17 chromatography; LS, light scattering; LAOS, large amplitude oscillating shear; SAOS, small

18 amplitude oscillating shear; LVR, linear viscoelastic region; NVR, nonlinear viscoelastic region;

19 DP, degree of polymerization

20 **Abstract:** This work investigated the chain structure and large amplitude oscillatory shear

21 (LAOS) rheological properties of waxy maize starch (WMS) at different growth periods and

22 established a motion model to clarify the evolution of chain structure. During the growth period

23 of 20-25 days, the apparent viscosity and dynamic moduli for WMS paste decreased, along with

24 a greater degree of nonlinearity. This could be correlated with an increasing branching degree of

25 starch due to more short-branched chains generated during growth. With the growth period

26 reaching 25 days, the apparent viscosity, dynamic moduli and zero-strain nonlinearity (Q_0) for

27 WMS increased and the b value deviated from 2 seriously, indicating obvious nonlinearity

28 accompanied by a weak stress overshoot and shear-thickening. This could be explained by the

29 growing length of branched chains and the rising content of B_3- and B_4-chains. Thus, this work

30 demonstrate LAOS rheology can be used as a new and effective method to characterize the chain

31 structural evolution of starch through monitoring the motion pattern of different starch chains

32 under shear conditions.

33

34 *Keywords*: Waxy maize starch; Amylopectin; Nonlinear rheology; Large amplitude oscillating

35 shear

36

1 Introduction

Starch is the main storage carbohydrate in plants. As a natural polymer material, starch has been widely used in diverse applications such as in food, pharmaceutical and chemical industries due to its advantages such as biodegradability, biocompatibility and low-price (Kochkina & Lukin, 2020). Starch consists of amylose and amylopectin, which form a semi-crystalline structure (Cai & Shi, 2010). According to amylose content, maize starch can be subdivided into high-amylose maize starch, normal maize starch and waxy maize starch. Waxy maize starch (WMS) is almost composed of amylopectin, which has a higher molecular weight and branching degree (Bertoft, 2013). The side chains of amylopectin can be divided into the outermost branchless A-chains, the backbone C-chains with a reductive end, and the B-chains that connect A-chains and C-chains, which can be further subdivided into B_1-chains, B_2-chains and B_3-chains depending on the degree of polymerization (Hizukuri, 1986; Madhusudhan & Tharanathan, 1996; Singh, Inouchi, & Nishinari, 2006). The understanding of starch chain structure is highly important as it is closely related to starch processability (Hsieh, Liu, Whaley, & Shi, 2019; Li, Su, Shi, Wang, & Chen, 2017). However, it is still highly challenging to analyze the chain structure of natural polymers, especially branched polymers. Commonly used spectroscopy and chromatographic analysis methods such as nuclear magnetic resonance (NMR), gel permeation chromatography (GPC), and light scattering (LS), all have certain limitations. For example, NMR cannot distinguish branched chains with length of six or more carbon atoms (Usmanov, 1991). GPC-LS can qualitatively explain the existence of branched chains by mean square radius of gyration, but the calculation of branching degree still needs to be based on the assumption of molecular structure (Wang, Kharchenko, Migler, & Zhu, 2004). Nowadays, there is still no direct method to determine the topological molecular structure of natural polymers. However, when the

60   molecular mass of starch branched chains exceed a critical value, chain entanglement results. In

61   this case, these branched chains can be called rheologically long branched chains. Specifically,

62   the rheological properties of the starch solution are sensitive to the molecular structure especially

63   branched-chain length, and thus rheology can be used for the qualitative and quantitative

64   characterization of starch chain structure (Liu et al., 2019b).

65   Rheological properties are important properties of starch-based food and materials, such as

66   during hot-extrusion 3D printing (Liu, Chen, Zheng, Xie, & Chen, 2020) and starch film (Silva-

67   Weissa, Bifani, Ihl, Sobralc, & Gómez-Guillénd, 2013), having great scientific and practical values in

68   understanding the starch structure and guiding starch processing (Yong et al., 2019). Starch paste

69   is a kind of pseudoplastic fluid with shear thinning behavior, as starch chains undergo

70   disentanglement and orientational arrangement under shear, leading to decreases in flow

71   resistance and viscosity (Ketthaisong, Suriharn, Tangwongchai, & Lertrat, 2014; Zhang, Li,

72   Zhang, Wei, & Fang, 2019). Dynamic rheology can effectively reflect the processing properties

73   and monitor the movement of molecular chains and the structural evolution of materials during

74   processing (Lee, Porcar, & Rogers, 2019). When starch paste is subjected to small-amplitude

75   shear, its solidity (elastic modulus) becomes more apparent, and its elastic modulus depends on

76   the degree of heterogeneity (Rodríguez-Hernández, Durand, Garnier, Tecante, & Doublier,

77   2006). Under large-strain shearing, the junctions connecting starch chains in starch paste are

78   broken and the chains are rearranged (Carmona, Ramírez, Calero, & Muñoz, 2014). Since strain

79   amplitude and frequency can be controlled independently under nonlinear viscoelastic

80   measurement, more information about the structure and properties of complex materials can be

81   obtained (Ghosh et al., 2019).

82   With the rapid development of precision instruments and computational simulations, large-

83   amplitude oscillating shear (LAOS) rheology has drawn much attention to probe the

84   microstructure of complex polymer systems (Duvarci, Yazar, & Kokini, 2017; Oliver, Scholten,

85   & van Aken, 2015). Hyun et al. (2009) investigated the nonlinear rheological properties of linear

86   and comb polystyrene and found two obvious peaks on the nonlinear viscoelasticity curve. The

87   peaks at low and high frequency correspond to the relaxation of backbone chains and branched

88   chains, respectively (Hyun & Wilhelm, 2009). They also reported that the relative intensity of

89   3rd harmonics ($I_{3/1}$) for linear polymers is proportional to the square of strain (γ_0^2), while the

90   slope of $I_{3/1}$ for branched polymers is normally less than 2. Therefore, the branching degree of

91   polymers can be measured quantitatively by the slope, and zero-strain nonlinearity can be used

92   for defining the nonlinearity of rheological behavior (Hyun et al., 2009). Oelschlaeger et al.

93   studied the microphase orientation/reorientation alignment behavior of two kinds of block

94   copolymers by LAOS rheology and found that the kinetics of orientation was strongly dependent

95   on the strain amplitude, and $I_{3/1}$ can be described by a stretched exponential function to

96   distinguish diblock copolymers and triblock copolymers with lamellar structure (Oelschlaeger et

97   al., 2010). By examining the interaction between fish gelatin and Arabic gum through LAOS

98   testing, Anvari et al. found the two gels had strong electrostatic attraction under a suitable pH

99   condition, thus forming a compact rigid network structure, which increased viscous dissipation

100   and led to a shift from elastic-dominated to viscous-dominated behavior (Anvari & Joyner,

101   2018). The main analysis methods of nonlinear rheology include Fourier-transform rheology,

102   Lissajous curves, stress decomposition, etc., and they can separate the structural characteristics

103   and flow behavior contained in a nonlinear stress response, which is highly useful for

104   understanding the molecular topology, molecular interactions, micromorphology and

105   crystallization of polymer fluids (Hyun et al., 2011).

106   In this study, WMS at different growth periods was studied by ion chromatography and

107   LAOS measurements to understand its chain-length distribution and nonlinear rheological

108   properties and to establish a correlation between them. Based on this, a motion model of starch

109   chains under different shear conditions was established. This study demonstrates the application

110   of nonlinear rheology in the analysis of starch chain structure and provides new knowledge

111   regarding the starch chain structural evolution during growth.

112 **2 Materials and methods**

113 **2.1 Materials**

114   Waxy maize of inbred line L5 was planted by the Zhong Luotan Experimental Base of the

115   Guangdong Academy of Agricultural Sciences (Guangzhou, China), and waxy maize seeds at

116   different growth periods (20 d, 25 d, 30 d and 35 d) were collected as experimental materials.

117   Amylose and amylopectin standards were purchased from the Heilongjiang Academy of

118   Agricultural Sciences (Harbin, China). Isoamylase (Cat. No. I5284, activity ≥3,000,000 U/mg)

119   from pseudomonas was purchased from Sigma-Aldrich Co., Ltd (Santa Clara, USA). Double

120   distilled water was used in this work. All reagents were of analytical grade and were used as

121   received without further purification.

122 **2.2 Sample preparations**

123   WMS was isolated from waxy maize following our previous method with minor

124   modification (Wang, Wang, Li, Chen, & Zhang, 2017). Waxy maize seeds at different growth

125   periods (20 d, 25 d, 30 d and 35 d) were selected and mixed with 0.45% (w/w) sodium

126 pyrosulfite at a weight ratio of 1:2. The mixture was smashed in a Waring Blender (HR 1727

127 Philips, Zhuhai, China) for 30 s, then stood at 4 °C for 12 h. The slurry was sieved by gauze and

128 sieve (75 μm) to eliminate fibers. Next, the slurry was centrifuged at 2800 g for 15 min and the

129 obtained precipitate was washed with sufficient water three times. Finally, the precipitate was

130 evenly mixed with absolute ethyl alcohol and filtered through a sieve (75 μm), and starch was

131 dried at 35 °C for 24 h. The prepared starch was named as starch 20, starch 25, starch 30 and

132 starch 35 according to its growth periods, respectively.

133 **2.3 Amylose content determination**

134   Amylose content of starch was determined using a previous method (Chen, Liang, Li,

135 Chen, & Xie, 2016; Liu, Zhang, Chen, Li, & Zheng, 2019a). The prepared starch (100 mg, dry

136 basis) was dispersed in 1 mol/L NaOH and then distilled water was added to achieve a 1 mg/mL

137 solution. Next, I_2/KI solution (0.0025 mol/L I_2 and 0.0065 mol/L KI) was used for amylose

138 complexation and the absorbance at 620 nm of the product was measured using a

139 spectrophotometer (Evolution 201, Thermo Scientific, USA). Amylose content was obtained

140 from a standard curve range from 0% to 100% that established using solutions of amylose and

141 amylopectin, and amylopectin content was equal to 100% minus amylose content.

142 **2.4 Amylopectin chain-length distribution**

143   The prepared starch (2 mg, dry basis) was dispersed in 0.5 mL of ethanol (95%) and 4.5

144 mL of distilled water. Then, the mixture was heated in boiling water for 60 min. Next, 2.5 mL of

145 the gelatinized starch paste was mixed with 125 μL of sodium acetate solution (600 mmol/L), 25

146 μL of sodium hydrazoic acid solution (2%, w/w) and 10 μL of isoamylase. After standing at 38

147 °C for 24 h, the pH was adjusted to 9.0 with ammonia solution (5%, w/w) and 375 μL of sodium

148 borohydride solution (2%, w/w) was added. The sample was equally divided into 600 μL per

149   tube and dried under vacuum at 25 °C. The dried sample was dissolved in 60 μL of NaOH

150   solution (1 mol/L) and diluted with 540 μL of distilled water, then centrifuged at 12000 rpm for

151   10 min. All supernatant prepared was uniformly mixed into one tube for analysis.

152   The amylopectin chain-length distribution was performed using a high-performance ion

153   chromatographer (HPIC) (ICS-5000, Dionex, USA) coupled with a pulsed amperometric

154   detection. The sample was eluted from an AP1 column (Dionex, USA) at a flow rate of 0.5

155   mL/min at 30 □ using a mixture of three eluents: 0.1 mol/L NaOH (eluent A), 0.1 mol/L NaOH

156   + 1 mol/L NaAc (eluent B), and water (eluent C). PAD signal was analyzed with the software

157   Peaknet (Dionex, USA) to obtained chain-length distribution (Kong, Bertoft, Bao, & Corke,

158   2008; Noda, Takahata, & Sato, 1995).

159

160   Table 1 Elution gradient (Kong, Bertoft, Bao, & Corke, 2008).

t / min	φ_A / %	φ_B / %	φ_C / %
0	55	10	35
8	40	25	35
25	35	30	35
65	20	45	35
75	55	10	35

161

162   **2.5 Rheological measurements**

163   Steady shear testing was performed on an MCR302 rheometer (Anton Paar, Austria) with a

164   parallel-plate geometry (25 mm diameter and 1 mm gap). WMS suspension of 4% (w/w, dry

165   basis) concentration was heated and stirred at 95 °C for 20 min, and then WMS paste was made

166   and preserved at 25 □. WMS paste was loaded and equilibrated at 25 □ for 5 min. Steady shear

167   testing in a range of 10^{-3}-10^{3} s^{-1} was conducted, and flow curves were acquired using

168   RheoCompass 1.21 software (Fang et al., 2019).

169   Strain sweep testing was performed on an ARES-G2 rheometer (TA Instruments, USA)

170   with a parallel-plate geometry (25 mm diameter and 1 mm gap). Similarly, 4% WMS paste was

171   loaded and equilibrated. Dynamic strain sweep testing in a range of 0.01%-1000% at 6.28 rad/s

172   was undertaken (Liu, Chen, Zheng, Xie, & Chen, 2020). Raw data under oscillation shear was

173   analyzed and processed by MITlaos (MATLAB Version, USA).

174   **2.6 Statistical analysis**

175   All tests were conducted at least in triplicate and the experimental data were analyzed

176   using SPSS Statistics 23.0 (IBM, USA). One-way analysis of variance was used to find the

177   significant difference by Duncan's test ($p \leq 0.05$).

178   **3 Results and discussion**

179   **3.1 Amylopectin content and amylopectin chain-length distribution**

180   Amylopectin has a higher density of branching attached by α-D-(1, 6)-glucosyl linkage in

181   the main α-D-(1,4)-glucosyl chain, which is mainly composed of A-chains, B-chains and C-

182   chains. Among them, there is only one C-chain in each amylopectin molecule, which has both a

183   non-reductive end and a reductive end. As branched chains, both A-chains and B-chains has only

184   non-reductive ends. Thus, enzymatic glucose chains produced by isoamylase also have multiple

185   hydroxyl groups, and they are dissociated into the form of anions in a strongly basic buffer.

186   Amylopectin chain-length distribution can be analyzed by measuring the retention time through

187   HPIC. As glucose chains of different length have different retention time, the chain-length

188   distribution can be determined according to the peak time and peak area in the chromatogram

189 (Kong et al., 2008). Generally, the chain-length distribution of starch can be divided into four

190 parts: A-chains (DP 6-12), B_1-chains (DP 13-24), B_2-chains (DP 25-36) and B_3-chains (DP>36)

191 (Madhusudhan et al., 1996; Singh et al., 2006). As presented in Table 1, the amylopectin content

192 and the B_2- and B_3-chain lengths of WMS all increased ($P \leq 0.05$) with a prolonged growth

193 period, while the length of B_1-chain, as the main type of amylopectin branch, increased first and

194 then decreased. The B_1-chain length of WMS increased notably during 20-25 d, and meanwhile,

195 amylopectin produced more short-branched chains. Nonetheless, when the growth period was

196 above 25 d, the degree of polymerization of branched chains further increased, leading to

197 increases in the B_2- and B_3-chain lengths.

198

199 Table 2 Amylopectin content and amylopectin chain-length distribution of WMS at different
200 growth periods.[A]

Sample	Amylopectin content / %	A-chains / %	B_1-chains / %	B_2-chains / %	B_3-chains / %
20	98.09±0.03[c]	20.6±0.2[a]	42.5±0.1[b]	18.9±0.1[c]	18.0±0.2[b]
25	98.18±0.02[c]	20.2±0.2[b]	42.9±0.1[a]	18.8±0.3[c]	18.1±0.2[b]
30	98.53±0.01[b]	20.0±0.2[b]	41.6±0.1[c]	20.0±0.2[b]	18.4±0.3[a]
35	98.89±0.02[a]	19.5±0.3[c]	41.2±0.2[d]	20.8±0.3[a]	18.5±0.2[a]

201 [A] The chain-length distribution is the percentage of individual chains in the total of the four chains.
202 Different letters above the same column indicate a significant difference ($P \leq 0.05$).

203

3.2 Steady shear characteristics

205 Fig. 1 shows the viscosity curves for WMS at different growth periods. Starch pastes are

206 typical pseudoplastic fluids with strong shear-thinning behavior. Regarding this, intertwined

207 starch chains were stretched under shear force and reoriented along the shear direction, causing

208 decreases in shear resistance and viscosity. In the low-shear rate region, the original structure of

209 WMS paste was destroyed, which was mainly caused by the unwinding of main chains, which

210 reduced the viscosity. With increasing shear rate, WMS paste flowed into the high-shear rate

211 region. In this case, the branched chains of starch also began to orientationally arrange under

212 shear, resulting in stronger shear-thinning behavior (Hyun et al., 2009). Compared with starch

213 20, the branching degree of starch 25 was higher with more short-branched chains, which limited

214 chain entanglement to some extent and thus resulted in lower viscosity of the starch paste. With

215 an even longer growth period, the DP of branched chains increased, contributing to chain

216 entanglement in the low-shear rate region and thus increasing the starch paste viscosity.

217 However, in the high-shear rate region, the long-branched chains (DP $\geq$25) also promoted the

218 unwinding and orientation of chains, and the formed structure was more sensitive to shear,

219 showing a strong non-Newtonian flow behavior with shear-thinning.

220
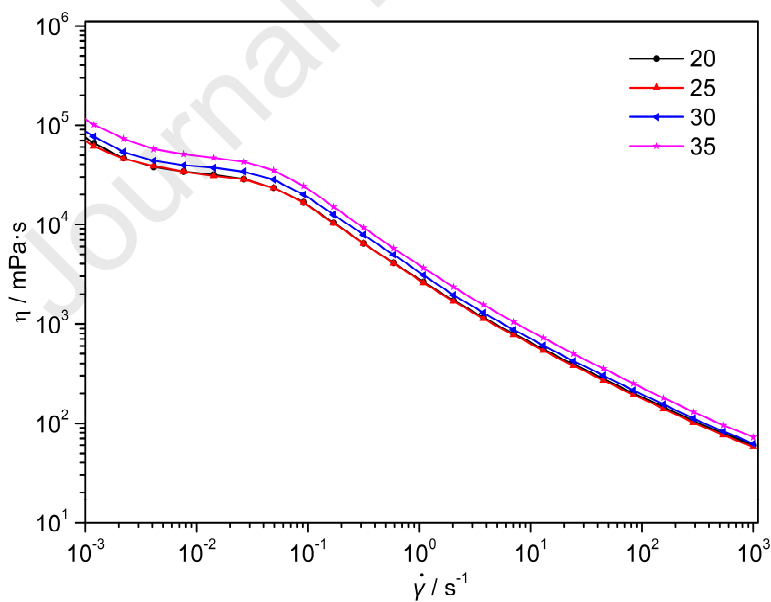
221

222   Fig. 1 Viscosity curves for WMS pastes at different growth periods.

223

3.3 Dynamic rheological properties

224

225   The dynamic viscoelasticity of WMS paste was determined by strain sweep testing. As

226 shown in Fig. 2, when the strain was 0.1-1%, the G' and G'' values of WMS paste did not change

227 with strain, indicating that the WMS paste was in the LVR and its network structure deformed

228 reversibly without destruction. Once the strain was greater than 1% and exceeded the LVR, G'

229 decreased with increasing strain, while G'' first rose slightly and then decreased abruptly. Once

230 WMS paste entered into NVR, its network structure began to collapse irreversibly, accompanied

231 by weakened chains interactions and mechanical strength of the paste, until reaching the flow

232 point where G' equals G''. In the strain sweep curves, G'' had a pronounced maximum value but

233 G' did not, showing a typical phenomenon of weak stress overshoot (Cloitre, Borrega, & Leibler,

234 2000; Hyun et al., 2011). This observation could indicate that the network junctions of WMS

235 paste were in a dynamic change process in the transition region. With increasing strain, the main

236 chains of starch were unwinding while partial long branched chains became entangled under

237 shearing. At this point, both the rates of creation and loss of junctions were positive, leading to a

238 balanced state. Afterwards, the creation rate was smaller than the loss rate, leading to the

239 weakening of chains entanglement. This further destroyed the cohesiveness of the network

240 structure, resulting in the occurrence of a yield point. From the dynamic strain sweep curves

241 (Fig. 2), both the G' and G'' values for starch 25 were smaller than those for starch 20, while the

242 G' and G'' values for starch 35 were the largest with an obvious stress overshoot. This was due to

243 the higher branching degree of starch 25 compared with that of starch 20. Nonetheless, its

244 branched chains were still not long enough to form entanglements, which led to a looser structure

245 of WMS paste with a larger molecular gap. In this case, the interactions between main chains

246 were restricted to some extent and the starch paste had reduced viscosity and rigidity as shown

247 by decreases in G' and G''. With the prolonging of the growth period, the length of branched

248 chains rose, and entanglement between branched chains occurred creating more junctions, which

249 increased the cohesiveness and the energy loss of the starch paste, as shown by increases in G'

250 and G''.

251
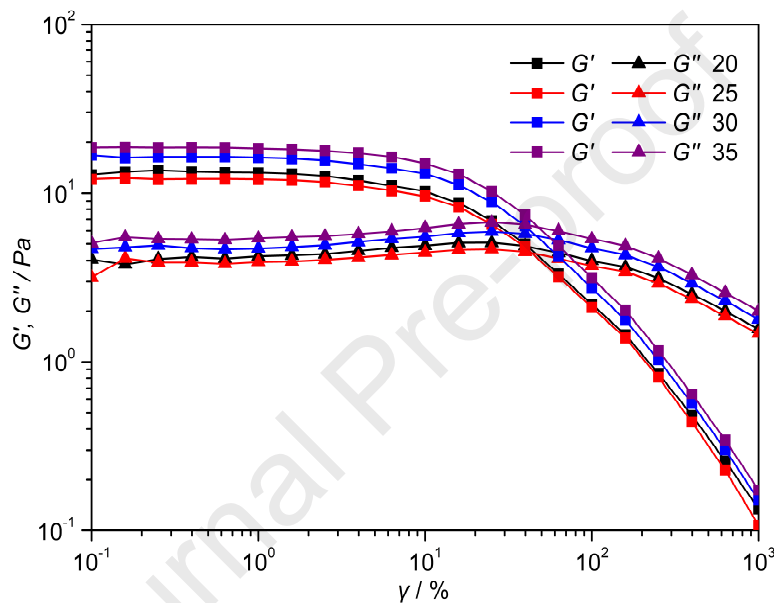
252

253   Fig. 2 Dynamic strain sweep curves for WMS pastes at different growth periods.

254

3.4 LAOS rheology analysis

256   Oscillatory shear testing is classified into two categories, namely small-amplitude

257 oscillatory shear (SAOS) and LAOS (Melito, Daubert, & Foegeding, 2012). When the applied

258 strain amplitude (γ_0) is small enough, the stress ($\sigma_{(t)}$) responds within the linear viscoelastic

259 region (LVR). With increasing strain at a certain frequency, the rheological behavior transits

260 from linear to nonlinear gradually and falls into the nonlinear viscoelastic region (NVR)

261 (Ptaszek, 2017). When the strain is low in the LVR, the storage modulus (G') and loss modulus

13

262 (G'') are independent of strain, and $\sigma_{(t)}$ is a sine function. When the strain exceeds a certain value,

263 the moduli begin to change with strain, and the waveform of $\sigma_{(t)}$ becomes distorted and

264 transforms into a non-sinusoidal function, in which case the common linear viscoelastic theory is

265 not applicable (Narsimhan, 1994). The main analysis methods for LAOS results proposed are

266 Fourier-transform rheology, Lissajous curves, and stress decomposition.

267   In Fourier-transform rheology, the relative strength of higher harmonics is taken as the

268 nonlinear metric, and the non-sinusoidal stress generated from LAOS testing is represented by

269 the Fourier series of elastic scaling (Eq. (1)) and viscous scaling (Eq. (2)) (Yan, Costanzo, Jeong,

270 Chang, & Vlassopoulos, 2016). In LAOS testing, $\sigma_{(t)}$ is a non-sinusoidal periodic function and

271 higher harmonics contribution appear under the Fourier transform, thus there are obvious signal

272 peaks at the ωt, $3\omega t$, $5\omega t$ … in the Fourier-transform rheology spectrum (Cogswell, 1991;

273 Wilhelm, Reinheimer, & Ortseifer, 1999). Wilhelm et al. studied the relative intensity of a high

274 harmonic and the first harmonic ($I_{n/1} = I_n / I_1$) and found that the nonlinear rheological behavior

275 of complex materials with different structures can be characteristic by $I_{3/1}$ (Wilhelm, Reinheimer,

276 Ortseifer, Neidhöfer, & Spiess, 2000). The nonlinear coefficient (Q) (Eq. (3)) in Fourier-

277 transform rheology provides strong evidence for the transformation from LVR to NVR.

278 Furthermore, the zero-strain nonlinearity (Q_0) (Eq. (5)) is defined as a constant value at relatively

279 small strain, which can effectively represent the inherent nonlinearity of complex fluids (Hyun et

280 al., 2009).

281      $\sigma(t, \omega, \gamma_0) = \gamma_0 \sum_{n=odd} [G'_n(\omega, \gamma_0) \sin(n\omega t) + G''_n(\omega, \gamma_0) \cos(n\omega t)]$ (1)

282      $\sigma(t, \omega, \gamma_0) = \dot{\gamma_0} \sum_{n=odd} [\eta'_n(\omega, \gamma_0) \sin(n\omega t) + \eta''_n(\omega, \gamma_0) \cos(n\omega t)]$ (2)

283      $Q = I_{3/1}/{\gamma_0}^2$ (3)

284      $\log I_{3/1} = a + b \log \gamma_0$ (4)

285 $$Q_0 = lim_{\gamma_0 \to 0} Q_{(\gamma_0)} = lim_{\gamma_0 \to 0} \left(I_{3/1}/\gamma_0{}^2 \right) \quad (5)$$

286   Where $\dot{\gamma}_0$ represents the maximum strain-rate, and G'_n and G''_n represent the elastic and

287   viscous moduli for the Nth harmonic, and η'_n and η''_n represent the apparent viscosity in phase

288   and out of phase for the Nth harmonic, and *I, Q* and Q_0 represent the relative intensity of high

289   harmonic, zero-strain nonlinearity and the slope of the fitting curve respectively.

290   The stress response in the NVR is processed by Fourier-transform to obtain the

291   contribution of higher harmonics, and it is found that the amplitude of the 3rd harmonic is high

292   and available. Therefore the nonlinear viscoelasticity of WMS paste at different growth periods

293   can be investigated by $I_{3/1}$ (Hyun et al., 2011). Fig. 3a shows that $I_{3/1}$ rose from 1% to 15% with

294   increasing strain. In LAOS testing, the branching degree of WMS can be measured quantitatively

295   by the slope *b* and Q_0, which were calculated by fitting using Eq. (4) and (5) (Fig. 3). As a rule,

296   the more the *b* value deviated from 2, the higher was the branching degree of WMS paste; and a

297   larger Q_0 value indicates a greater degree of the inherent nonlinearity. The prolonging of the

298   growth period was found to decrease *b* from 0.7384 to 0.4671 (Table 3), which deviated from 2

299   largely, while Q_0 increased from 0.0017 to 0.0087 (Table 3). This indicates that the inherent

300   nonlinear characteristic of WMS paste became more significant. These results were ascribed to

301   increases in amylopectin content and the length of branched chains in WMS. In this case, there

302   was an unstable network structure in WMS paste, which was prone to show nonlinearity under

303   LAOS testing.

304

305

306

307   Fig. 3 Curves of $I_{3/1}$ and Q for WMS pastes at different growth periods.

308

309   Table 3 Fitting parameters for WMS pastes at different growth periods.

20	25	30	35

|				
b	0.7384	0.5998	0.5913	0.4671
Q_0	0.0017	0.0036	0.0039	0.0087

310

311   Nonlinear stress response can be probed by associated Lissajous curves, where the

312 obtained stress curve can be easily separated into the strain function and the shear rate function

313 to display the elastic contribution and the viscous contribution of the nonlinear response,

314 respectively (Ptaszek, et al., 2016). A Lissajous curve eliminates the influence of time variables,

315 and different Lissajous curves are generated with different frequency and strain. Notably, the

316 elastic and viscous Lissajous plots can be represented as a function of strain (Fig. 4a) and strain-

317 rate (Fig. 4b), and the dotted line indicates elastic stress and viscous stress, respectively (Anvari

318 et al., 2018). All elastic and viscous Lissajous plots for WMS pastes at different growth periods

319 were elliptic at 1% strain, and the elastic and viscous stress were in a straight line, indicating

320 ideal viscoelastic behavior. With increasing strain, the Lissajous plots changed from ellipse to

321 parallelogram with distortion, and the elastic and viscous stresses became bent, indicating

322 nonlinear viscoelasticity with the appearance of high harmonic contribution. In the high strain

323 range, the slope of elastic stress increased significantly, suggesting strain-stiffening behavior of

324 the WMS paste (Fig. 4a), while the slope of viscous stress decreased with shear-thinning in the

325 high strain-rate range (Fig. 4b).

326

327

328
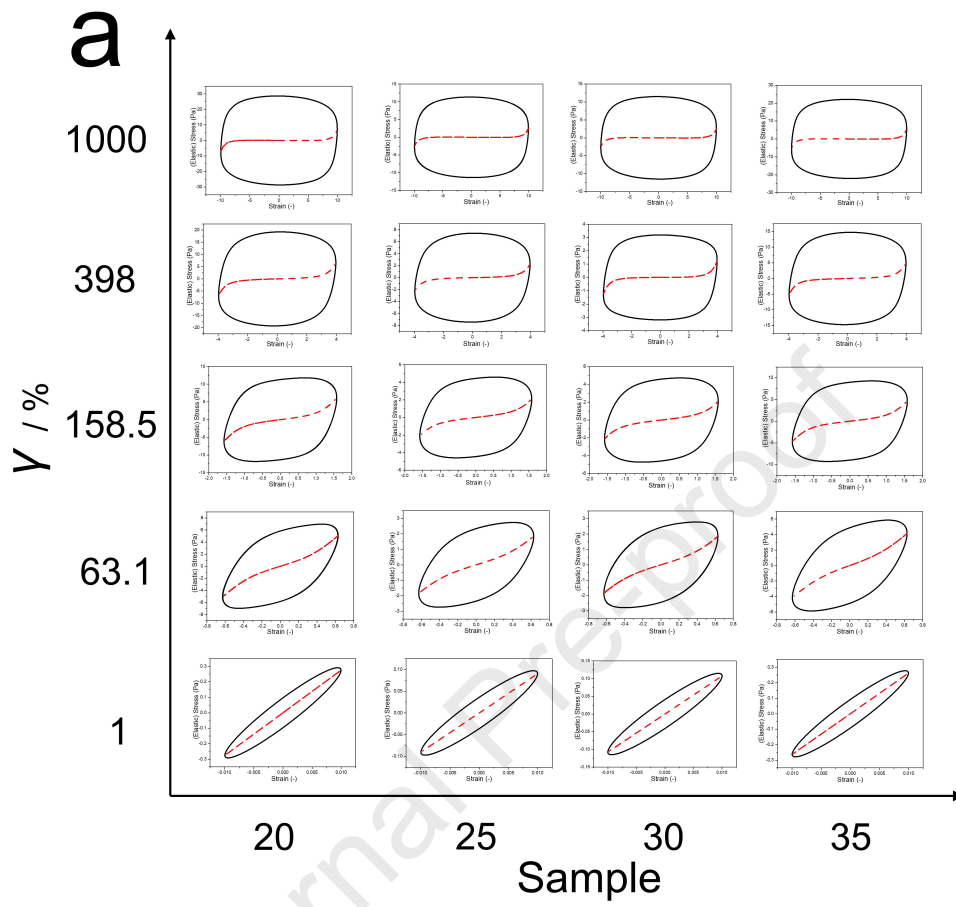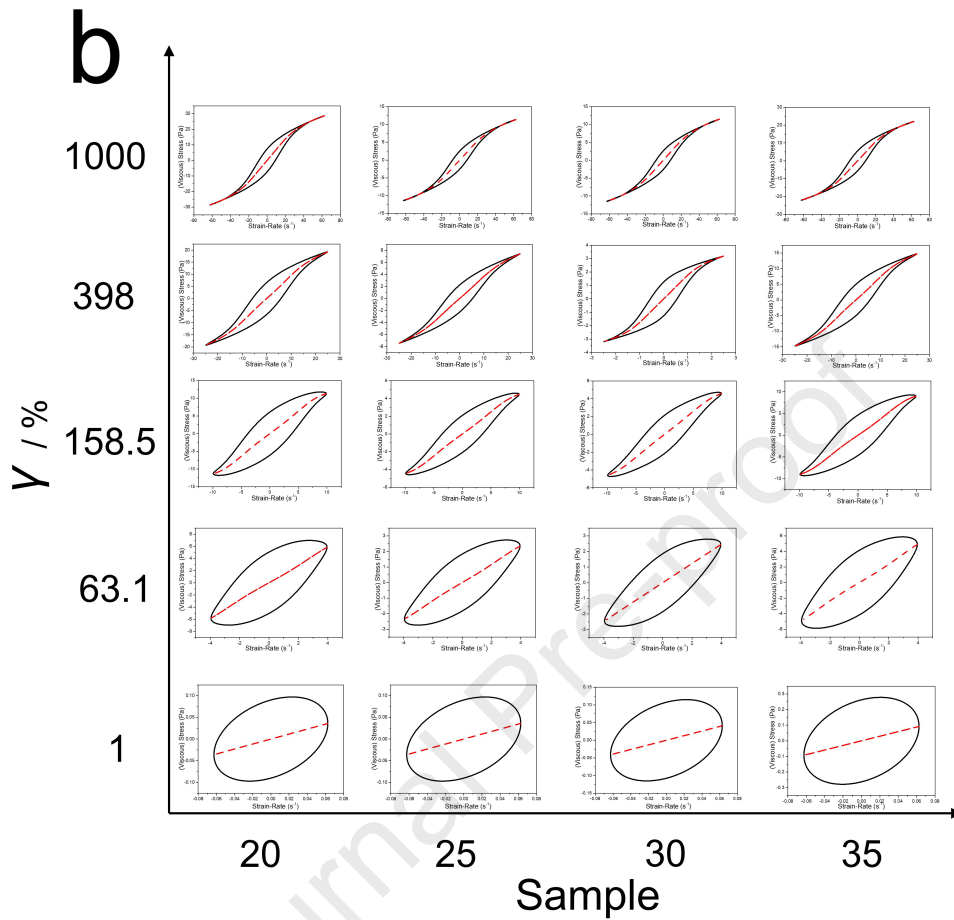
Fig. 4 Lissajous plots for WMS pastes at different growth periods. (a) the elastic parts; (b) the

330   viscous parts.

331

332   G'_L and G'_M are determined as the secant modulus at the maximum and zero strains.

333 Similarly, η'_L and η''_M are determined as the dynamic viscosity at the maximum and zero shear

334 rates (Ewoldt, Hosoi, & McKinley, 2008). As can be seen from Table 4, the G'_L and G'_M, η'_L and

335 η'_M values for WMS pastes at different growth periods were equal at 1% strain, which also

336 suggests that the tests were within the LVR. When the strain exceeded 1%, the G'_L and G'_M, η'_L

337 and η'_M value began to be different, and the tests were beyond the LVR, resulting in strain-

338 stiffening/softening and shear-thickening/thinning. Under the same strain, the LAOS parameters

19

339   for WMS paste decreased first and then increased with a longer growth period. Among them, the

340   parameters for starch 25 were the smallest, in agreement with the strain sweep results. Compared

341   with that of starch 20, the amylopectin content of starch 25 increased but its branched chains

342   were relatively short, thus the presence of short-branched chains without entanglements inhibited

343   interactions between main chains and there were fewer junctions in the network structure,

344   leading to lower rigidity and viscosity. When the growth period was more than 25 d, the length

345   of branched chains increased significantly, which led to enhanced chain interactions, resulting in

346   increased elastic moduli and viscosity of the starch paste.

347

348   Table 4 LAOS parameters for WMS pastes at different growth periods.

Sample	Viscoelasticity	$\gamma = 1\%$	$\gamma = 63.1\%$	$\gamma = 158.5\%$	$\gamma = 398\%$	$\gamma = 1000\%$
20	$G_M{'}$ / Pa	27.606±0.031	4.679±0.016	1.245±0.015	0.154±0.002	-0.030±0.001
	$G_L{'}$ / Pa	27.606±0.031	8.036±0.019	3.860±0.018	1.662±0.004	0.741±0.012
	$\eta_M{'}$ / Pa·s	1.541±0.018	1.329±0.010	1.179±0.013	0.891±0.008	0.689±0.018
	$\eta_L{'}$ / Pa·s	1.541±0.018	1.477±0.011	1.141±0.014	0.773±0.019	0.458±0.014
25	$G_M{'}$ / Pa	9.042±0.022	1.825±0.015	0.474±0.013	0.028±0.001	-0.014±0.001
	$G_L{'}$ / Pa	9.042±0.022	2.907±0.017	1.322±0.010	0.569±0.018	0.253±0.007
	$\eta_M{'}$ / Pa·s	0.576±0.017	0.547±0.009	0.459±0.011	0.348±0.010	0.269±0.009
	$\eta_L{'}$ / Pa·s	0.576±0.017	0.593±0.002	0.449±0.014	0.298±0.009	0.182±0.009
30	$G_M{'}$ / Pa	10.746±0.023	1.798±0.014	0.469±0.012	0.031±0.002	-0.023±0.001
	$G_L{'}$ / Pa	10.746±0.023	2.945±0.016	1.357±0.014	0.617±0.012	0.263±0.010
	$\eta_M{'}$ / Pa·s	0.652±0.018	0.616±0.009	0.495±0.010	0.413±0.014	0.280±0.010

η_L' / Pa·s	0.652±0.018	0.617±0.013	0.463±0.008	0.319±0.014	0.184±0.005
G_M' / Pa	26.331±0.027	4.232±0.012	0.951±0.011	0.102±0.008	-0.024±0.001
G_L' / Pa	26.331±0.027	6.598±0.018	2.950±0.017	1.265±0.017	0.561±0.0013
η_M' / Pa·s	1.472±0.012	1.103±0.010	0.907±0.016	0.689±0.012	0.527±0.011
η_L' / Pa·s	1.472±0.012	1.237±0.013	0.906±0.017	0.592±0.012	0.353±0.007

349   To investigate the change in elastic modulus and instantaneous viscosity of materials under

350 shear, Ewoldt et al. (2008) proposed to use the ratios of strain-stiffening (S) (Eq. (6)) and shear-

351 thickening (T) (Eq. (7)) to further understand if it is strain-stiffening (S >0) or softening (S <0)

352 and if it is shear-thickening (T >0) or thinning (T <0) under nonlinear intracycle shearing

353 (Ewoldt et al., 2008; Hyun et al., 2011;Carmona et al., 2014; Zhang et al., 2019).

354    $S = (G'_L - G'_M)/G'_L$ (6)

355    $T = (\eta'_L - \eta'_M)/\eta'_L$ (7)

356   As shown in Fig. 5, all the S values for WMS paste was a positive value and increased with

357 increasing strain, showing strong shear-stiffening behavior. During dynamic shearing, the

358 network structure of WMS paste was in the reversible deformation without destruction in the

359 LVR, while WMS paste underwent plastic deformation when the strain exceeded the yield point.

360 In the case, molecular chains were aligned along the strain direction, and hydrogen-bonding

361 interactions occurred between starch chains, which increased the ordering and deformation-

362 resistance. Thus, the S curve continued to rise but the slope gradually decreased. Besides, the

363 interior structure of WMS paste was destroyed and reorganized constantly to form more stable

364 and a strong network structure under shearing, further contributing to stress-hardening. On the

365 other hand, the T value for WMS paste increased first and then decreased and T was a positive

366 value only at 63.1% strain, suggesting WMS paste showed intracycle shear-thickening only at

367   63.1% strain but shear-thinning under other strain conditions. Compared with other starch

368   samples, the S value for starch 35 was the maximum at 63.1% strain due to its relatively high

369   content of amylopectin and long-branched chains, in agreement with the strain sweep results.

370   Regarding this phenomenon, loose and irregular long branched chains had a shorter relaxation

371   time than main chains so that it had enough time to move and re-entangle, resulting in increased

372   viscosity and shear-thickening. With a continuous increase in strain, main chains and branched

373   chains in WMS paste were rearranged orientationally under shearing and the entanglements

374   between starch chains weakened, leading to decreased viscosity with shear-thinning behavior.

375

376

377   Fig. 5 The S and T curves of WMS at different growth periods.

378   The total stress obtained in oscillating shear testing can be decomposed into two parts

379   (elastic stress and viscous stress). Cho et al. used Chebyshev polynomials to perform the

380   orthogonal decomposition of total stress (Eq. (8) and (9)), where the Chebyshev coefficient

381   nicely explains the contribution of higher harmonics and is closely related to the elastic and

22

382   viscous stresses in nonlinear rheology (Cho, Hyun, Ahn, & Lee, 2005). The strain-

383   stiffening/softening and shear-thickening/thinning are judged by the sign of the third-order

384   Chebyshev coefficients, and e_3 >0 and v_3 >0 indicate intracycle strain-stiffening and shear-

385   thickening, respectively, whereas e_3 <0 and v_3 <0 correspond to intracycle strain-softening and

386   shear-thinning, which further clarified the motion of molecular chains under large-strain

387   conditions, including directional arrangement and reconstruction (Cho et al., 2005; Ewoldt et al.,

388   2008), and it is similar to the case shown by Fourier-transform rheology (Cho et al., 2005).

389    $$\sigma'(\frac{\gamma}{\gamma_0}) = [\sigma(\gamma,\dot{\gamma}) - \sigma(-\gamma,\dot{\gamma})]/2 = \gamma_0 \sum_{n=odd} e_n(\omega,\gamma_0) T_n(\frac{\gamma}{\gamma_0}) \qquad (8)$$

390    $$\sigma''(\frac{\dot{\gamma}}{\dot{\gamma}_0}) = [\sigma(\gamma,\dot{\gamma}) - \sigma(\gamma,-\dot{\gamma})]/2 = \dot{\gamma}_0 \sum_{n=odd} v_n(\omega,\gamma_0) T_n(\frac{\dot{\gamma}}{\dot{\gamma}_0}) \qquad (9)$$

391   Where σ' and σ'' represent elastic stress and viscous stress respectively, and the e_n and v_n

392   represent the Chebyshev coefficients at Nth order, T_n represents the Chebyshev functions.

393   Fig. 6 provides that e_3 was a positive value for all the samples, showing strong shear-

394   stiffening behavior. And, v_3 was a positive value only at 63.1% strain but negative under other

395   strain conditions, which was consistent with the results in Fig. 5.

396

397   Fig. 6 e_3 and v_3 curves for WMS pastes at different growth periods.

398

399 **3.5 Motion model of WMS chains**

400   In the steady shear testing, the apparent viscosity change of WMS paste was divided into

401 two parts, namely the unwinding and reorientation of main chains under weak shear and the

402 unwinding and reorientation of main chains and branched chains under intensive shear, as

403 reflected by its strong shear-thinning behavior. In dynamic shear testing, when the strain

404 exceeded the yield point, the WMS paste structure began to break down and reconstruct, and the

405 test entered the NVR. Besides, from LVR to NVR, WMS paste appeared to show a weak stress

406 overshoot and shear-thickening behavior because the long branched chains with a shorter

407 relaxation time had enough time to re-entangle under shearing, which led to increased loss

408 modulus. Once WMS paste was subject to strain that is large enough, main chains and branched

409 chains of amylopectin were unwound under shearing and they changed from random coils to an

410 orientated state following the damage and restructuration of the starch structure. This resulted in

24

411   the formation of a more stable and stronger network structure with intracycle strain-stiffening.

412   Meanwhile, the entanglement or hooking effect of starch chains was weakened, leading to

413   decreased instantaneous viscosity with intracycle shear-thinning behavior. Most short-branched

414   chains of starch 25 were not long enough to form entanglements and thus chain interactions were

415   restricted, resulting in decreased viscosity and moduli. When the growth period was longer than

416   25 d, the DP of branched chains increased and more starch chains intertwined, leading to

417   increased viscosity and moduli of the WMS paste. This reveals obvious nonlinearity

418   accompanied by a weak stress overshoot and shear-thickening behavior. Therefore, the structural

419   evolution of WMS chains can be clearly shown by the nonlinear rheological data.
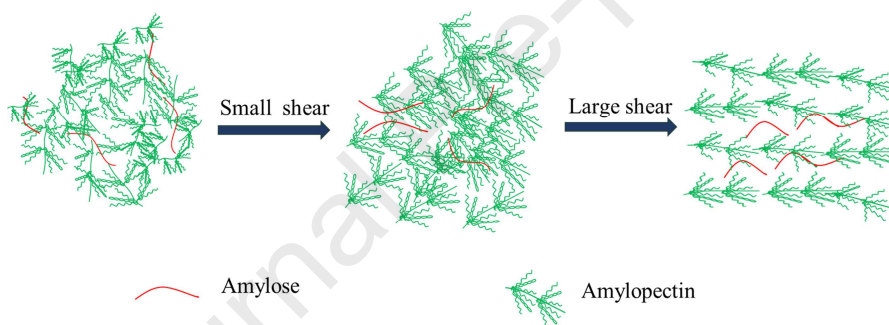
420

421   Fig. 7 Motion model of WMS chains under shearing

4 Conclusion

422

423   We investigated that the amylopectin content and branched chains of WMS increased with

424   prolonged growth period, in which long branched chains (DP $\geq$25) improved the apparent

425   viscosity and dynamic moduli of the starch paste, while short branched chains did the reverse. In

426   the steady shear testing, compared with main chains, long branched chains underwent unwinding

427   and reorientation accompanied by strong shear-thinning behavior at high shear rate. In the

428   dynamic shear testing, long branched chains re-entangled in the strain transition region, leading

429   to a weak stress overshoot and shear-thickening (T >0). When WMS paste was subjected to

25

430 LAOS, it showed intracycle strain-stiffening and shear-thinning behaviors, while the nonlinearity

431 of WMS paste became more distinct with increasing amylopectin content and branched chains

432 length. In all, nonlinear rheology can be used as a new way to characterize the structural

433 evolution of starch chains.

Conflict of interests

435 The authors declare to have no conflict of interests.

Acknowledgment

References

441 Anvari, M., & Joyner, H. S. (2018). Effect of fish gelatin and gum arabic interactions on concentrated

442 emulsion large amplitude oscillatory shear behavior and tribological properties. *Food

443 Hydrocolloids, 79*, 518-525.

444 Bertoft, E. (2013). On the Building Block and Backbone Concepts of Amylopectin Structure. *Cereal

445 Chemistry, 90*, 294-311.

446 Cai, L., & Shi, Y. C. (2010). Structure and digestibility of crystalline short-chain amylose from

447 debranched waxy wheat, waxy maize, and waxy potato starches. *Carbohydrate Polymers, 79*,

448 1117-1123.

449 Carmona, J. A., Ramírez, P., Calero, N., & Muñoz, J. (2014). Large amplitude oscillatory shear of xanthan

450 gum solutions. Effect of sodium chloride (NaCl) concentration. *Journal of Food Engineering,

451 126*, 165-172.

452 Chen, J., Liang, Y., Li, X., Chen, L., & Xie, F. (2016). Supramolecular structure of jackfruit seed starch

453   and its relationship with digestibility and physicochemical properties. *Carbohydrate Polymers,*

454   *150*, 269-277.

455   Cho, K. S., Hyun, K., Ahn, K., & Lee, S. (2005). A geometrical interpretation of large amplitude

456   oscillatory shear response. *Journal of Rheology, 49*, 747-758.

457   Cloitre, M., Borrega, R., & Leibler, L. (2000). Rheological aging and rejuvenation in microgel pastes.

458   *Physical Review Letters, 85*, 4819-4822.

459   Cogswell, F. N. (1991). Melt Rheology and its Role in Plastic Processing: Theory and Applications.

460   *Journal of Non-Newtonian Fluid Mechanics, 39*, 407-409.

461   Duvarci, O. C., Yazar, G., & Kokini, J. L. (2017). The comparison of LAOS behavior of structured food

462   materials (suspensions, emulsions and elastic networks). *Trends in Food Science & Technology,*

463   *60*, 2-11.

464   Ewoldt, R., Hosoi, A., & McKinley, G. (2008). New measures for characterizing nonlinear viscoelasticity

465   in large amplitude oscillatory shear. *Journal of Rheology, 52*, 1427-1458.

466   Fang, Y., Tuncil, X., Luo, X. T., & Bruce. (2019). Shear-thickening behavior of gelatinized waxy starch

467   dispersions promoted by the starch molecular characteristics. *International Journal of Biological*

468   *Macromolecules, 121*, 120-126.

469   Ghosh, A., Chaudhary, G., Kang, J. G., Braun, P. V., Ewoldt, R. H., & Schweizer, K. S. (2019). Linear and

470   nonlinear rheology and structural relaxation in dense glassy and jammed soft repulsive pNIPAM

471   microgel suspensions. *Soft Matter, 15*, 1038-1052.

472   Hizukuri, S. (1986). Polymodal distribution of the chain lengths of amylopectins, and its significance.

473   *Carbohydrate Research, 147*, 342-347.

474   Hsieh, C. F., Liu, W., Whaley, J. K., & Shi, Y. C. (2019). Structure, properties, and potential applications

475   of waxy tapioca starches – A review. *Trends in Food Science & Technology, 83*, 225-234.

476   Hyun, K., & Wilhelm, M. (2009). Establishing a New Mechanical Nonlinear Coefficient Q from FT-

477   Rheology: First Investigation of Entangled Linear and Comb Polymer Model Systems.

478   *Macromolecules, 42*, 411-422.

479   Hyun, K., Wilhelm, M., Klein, C. O., Cho, K. S., Nam, J. G., Ahn, K. H., et al. (2011). A review of

480   nonlinear oscillatory shear tests: Analysis and application of large amplitude oscillatory shear

481   (LAOS). *Progress in Polymer Science, 36*, 1697-1753.

482   Ketthaisong, D., Suriharn, B., Tangwongchai, R., & Lertrat, K. (2014). Changes in physicochemical

483   properties of waxy corn starches after harvest, and in mechanical properties of fresh cooked

484   kernels during storage. *Food Chemistry, 151*, 561-567.

485   Kochkina, N. E., & Lukin, N. D. (2020). Structure and properties of biodegradable maize starch/chitosan

486   composite films as affected by PVA additions. *International Journal of Biological*

487   *Macromolecules, 157*, 377-384.

488   Kong, X., Bertoft, E., Bao, J., & Corke, H. (2008). Molecular structure of amylopectin from amaranth

489   starch and its effect on physicochemical properties. *International Journal of Biological*

490   *Macromolecules, 43*, 377-382.

491   Lee, J. C. W., Porcar, L., & Rogers, S. (2019). Unveiling Temporal Nonlinear Structure-Rheology

492   Relationships under Dynamic Shearing. *Polymers, 11*, 1189-1205.

493   Li, Y., Su, X., Shi, F., Wang, L., & Chen, Z. (2017). High-temperature air--fluidization-induced changes in

494   the starch texture, rheological properties, and digestibility of germinated brown rice. *Starch -*

495   *Stärke, 69*, 1-10.

496   Liu, K., Zhang, B., Chen, L., Li, X., & Zheng, B. (2019a). Hierarchical structure and physicochemical

497   properties of highland barley starch following heat moisture treatment. *Food Chemistry, 271*,

498   102-108.

499   Liu, S., Xiao, Y., Shen, M., Zhang, X., Wang, W., & Xie, J. (2019b). Effect of sodium carbonate on the

500   gelation, rheology, texture and structural properties of maize starch-Mesona chinensis

501   polysaccharide gel. *Food Hydrocolloids, 87*, 943-951.

502   Liu, Z., Chen, H., Zheng, B., Xie, F., & Chen, L. (2020). Understanding the structure and rheological

503   properties of potato starch induced by hot-extrusion 3D printing. *Food Hydrocolloids, 105*,

504   105812.

505   Madhusudhan, B., & Tharanathan, R. N. (1996). Structural studies of linear and branched fractions of

506   chickpea and finger millet starches. *Carbohydrate Research, 284*, 101-109.

507   Melito, H. S., Daubert, C. R., & Foegeding, E. A. (2012). Validation of a large amplitude oscillatory shear

508   protocol. *Journal of Food Engineering, 113*, 124-135.

509   Narsimhan, G. (1994). Rheological methods in food process engineering: By James F. Steffe. *Journal of

510   Food Engineering, 23*, 249-250.

511   Noda, T., Takahata, Y., & Sato, T. (1995). Distributions of the Amylopectin Chain Length of Sweet

512   Potatoes Differing in Stages of Development, Tissue Zone and Variety. *Nippon Shokuhin Kagaku

513   Kogaku Kaish, 42*, 200-206.

514   Oelschlaeger, C., Gutmann, J. S., Wolkenhauer, M., Spiess, H. W., Knoll, K., & Wilhelm, M. (2010).

515   Kinetics of Shear Microphase Orientation and Reorientation in Lamellar Diblock and Triblock

516   Copolymer Melts as Detected via FT-Rheology and 2D-SAXS. *Macromolecular Chemistry &

517   Physics, 208*, 1719-1729.

518   Oliver, L., Scholten, E., & van Aken, G. A. (2015). Effect of fat hardness on large deformation rheology

519   of emulsion-filled gels. *Food Hydrocolloids, 43*, 299-310.

520   Ptaszek, P. (2017). Large Amplitude Oscillatory Shear (LAOS) Measurement and Fourier-Transform

521   Rheology: Application to Food. In J. Ahmed, P. Ptaszek & S. Basu (Eds.), *Advances in Food

522   Rheology and Its Applications* (pp. 87-123): Woodhead Publishing.

523   Ptaszek, P., Kabziński, M., Ptaszek, A., Kaczmarczyk, K., Kruk, J., & Bieńczak, A. (2016). The analysis

524   of the influence of xanthan gum and apple pectins on egg white protein foams using the large

525   amplitude oscillatory shear method. *Food Hydrocolloids, 54*, 293-301.

526   Rodríguez-Hernández, A. I., Durand, S., Garnier, C., Tecante, A., & Doublier, J. L. (2006). Rheology-

527   structure properties of waxy maize starch–gellan mixtures. *Food Hydrocolloids, 20*, 1223-1230.

528   Silva-Weissa A., Bifani V., Ihl M., Sobralc P.J.A., & Gómez-Guillénd M.C. (2013). Structural properties

529   of films and rheology of film-forming solutions based on chitosan and chitosan-starch blend

530   enriched with murta leaf extract. *Food Hydrocolloids, 31*, 458-466.

531

532 Singh, N., Inouchi, N., & Nishinari, K. (2006). Structural, thermal and viscoelastic characteristics of

533   starches separated from normal, sugary and waxy maize. *Food Hydrocolloids, 20*, 923-935.

534 Usmanov, T. I. (1991). NMR spectroscopy of polysaccharide derivatives and their molecular structure.

535   Review. *Polymer Science U.S.S.R., 33*, 611-635.

536 Wang, H., Wang, Z., Li, X., Chen, L., & Zhang, B. (2017). Multi-scale structure, pasting and digestibility

537   of heat moisture treated red adzuki bean starch. *International Journal of Biological*

538   *Macromolecules, 102*, 162-169.

539 Wang, W., Kharchenko, S., Migler, K., & Zhu, S. (2004). Triple-detector GPC characterization and

540   processing behavior of long-chain-branched polyethylene prepared by solution polymerization

541   with constrained geometry catalyst. *Polymer, 45*, 6495-6505.

542 Wilhelm, M., Reinheimer, P., & Ortseifer, M. (1999). High sensitivity Fourier-transform rheology.

543   *Rheologica Acta, 38*, 349-356.

544 Wilhelm, M., Reinheimer, P., Ortseifer, M., Neidhöfer, T., & Spiess, H. W. (2000). The crossover between

545   linear and non-linear mechanical behaviour in polymer solutions as detected by Fourier-transform

546   rheology. *Rheologica Acta, 39*, 241-246.

547 Yan, Z. C., Costanzo, S., Jeong, Y., Chang, T., & Vlassopoulos, D. (2016). Linear and Nonlinear Shear

548   Rheology of a Marginally Entangled Ring Polymer. *Macromolecules, 49*, 1444-1453.

549 Yong, S. P., Qiu, T. X., Xiao, M. B., Zhang, H. Q., & Chen. (2019). Evaluation studies on effects of

550   pectin with different concentrations on the pasting, rheological and digestibility properties of corn

551   starch. *Food Chemistry, 274*, 319-323.

552 Zhang, Y. F., Li, J. B., Zhang, Z. Y., Wei, Q. S., & Fang, K. (2019). Rheological law of change and

553   conformation of potato starch paste in an ultrasound field. *Journal of Food Measurement and*

554   *Characterization, 13*, 1695–1704.

555

Highlights

- Nonlinear rheology was used in the insight into waxy maize starch chains

- Branched chains (DP ≥25) improved the apparent viscosity and dynamic moduli

- Amylopectin content and B-chains length increased its nonlinearity

- Motion model of WMS chains under shearing was established

– Declaration of Interest–

An insight into the structural evolution of waxy maize starch chains during growth based on nonlinear rheology

Zipeng Liu [a], Ling Chen [a,**], PingPing Bie [a], Fengwei Xie [b, c], and Bo Zheng [a,*]

[a] *Ministry of Education Engineering Research Center of Starch & Protein Processing, Guangdong Province Key Laboratory for Green Processing of Natural Products and Product Safety, School of Food Science and Engineering, South China University of Technology, Guangzhou 510640, China*

[b] *International Institute for Nanocomposites Manufacturing (IINM), WMG, University of Warwick, Coventry CV4 7AL, United Kingdom*

[c] *School of Chemical Engineering, The University of Queensland, Brisbane, Qld 4072, Australia*

The authors declare that there is no conflict of interest regarding the publication of this article.